

Bayesian Lorentzian profile fitting using Markov-Chain Monte Carlo: An observer's approach

M. Gruberbauer¹, T. Kallinger¹, and W.W. Weiss¹

Institute for Astronomy (IfA), University of Vienna, Türkenschanzstrasse 17, A-1180 Vienna,
e-mail: last_name@astro.univie.ac.at

Received / Accepted

ABSTRACT

Aims. Investigating stochastically driven pulsation puts strong requirements on the quality of (observed) pulsation frequency spectra, such as the accuracy of frequencies, amplitudes, and mode life times and – important when fitting these parameters with models – a realistic error estimate which can be quite different to the formal error. As has been shown by other authors, the method of fitting Lorentzian profiles to the power spectrum of time-resolved photometric or spectroscopic data via the Maximum Likelihood Estimation (MLE) procedure delivers good approximations for these quantities. We, however, intend to demonstrate that a conservative Bayesian approach allows to treat this problem in a more consistent way.

Methods. We derive a conservative Bayesian treatment for the probability of Lorentzian profiles being present in a power spectrum and describe its implementation via evaluating the probability density distribution of parameters by using the Markov-Chain Monte Carlo (MCMC) technique. In addition, we compare the results obtained by Appourchaux et al. (2008), who used the MLE technique, on the CoRoT* data of HD 49933 to our Bayesian approach.

Results. Rather than using a “best-fit” procedure like MLE, which can only deliver formal uncertainties, our procedure samples and approximates the actual probability distributions for all parameters involved. Moreover, it helps avoiding shortcomings that make the MLE treatment susceptible to the complexity of a model that is fitted to the data. This is especially relevant when analysing solar-type pulsation in other stars than the Sun where the observations usually have lower quality and we illustrate this claim in a reassessment of the pulsation of HD 49933.

Key words. stars: oscillations – methods: statistical – stars: individual: HD 49933

1. Introduction

Our understanding of the Sun's structure has been revolutionised over the last three decades by helioseismology, which allows to investigate the solar interior by making use of the acoustic modes observed on the solar surface. As ultra-precise rapid photometry from space and high-precision radial velocity measurements became available, low degree, high radial order p modes were reported for several main-sequence and sub-giant stars (see e.g., Bedding & Kjeldsen 2006). The damped and stochastically excited (solar-type) oscillations, typical for those stars, are induced by turbulent convection in the outer stellar layers and provide information about the stellar structure by using strategies successfully applied to the Sun. One of these strategies is to compare the observed frequencies and their characteristic spacings to those derived from stellar models. For main-sequence and sub-giant stars the characteristic frequency spacings, such as the asymptotic large and small frequency separations, are large compared to the observational uncertainties. Even small deviations from the asymptotic relation caused by more local phenomena in the stellar interior can be studied. An important aspect of such an analysis is the reliability and accuracy of the observed stellar frequency spectrum. Even a few incorrectly identified frequencies, i.e., frequencies that are not intrinsic to the star but an artefact of the data processing or of instrumental origin, complicate significantly

the analysis or can even lead to a misinterpretation of the observations. The importance of *reliability* in comparison to *size* of the observed frequency spectrum needs to be emphasised. Of similar relevance are realistic frequency uncertainties, because they restrict model parameter determination. Due to limited data quality of non solar observations, fits often result in very uncertain parameter determinations or do not even converge when all parameters are treated independently. To reduce the number of free parameters to be fitted, it is common practice to couple individual parameters. From geometrical considerations one can expect, e.g., a fixed amplitude ratio between modes of different degree. This measure might stabilize the fit or even allows to detect modes almost hidden in the noise. On the other hand, this assumption does not hold if the stellar surface is strongly inhomogeneous (e.g. due to stellar activity) or can significantly hinder the model fitting if a hidden mode is not present.

Some Bayesian treatments of solar-type oscillations have already been suggested (e.g., Brewer et al. 2007). The implementation of Markov-Chain Monte Carlo techniques for a Bayesian analysis of Lorentzian profiles has also already been described. Benomar (2008), for instance, suggests models that include rotational splitting and additional modes that are expected from theory, but are not clearly discernible in the power spectrum. This of course does not mean that there is no formal evidence for these model details in the data. However, to test the evidence for each single Lorentzian profile component in a p -mode spectrum, we argue for a more general approach. Rather than fitting different complex models as a whole to the observations and comparing the results, we formulate solar-type p -mode spectrum fitting as

* The CoRoT (COncvection, ROTation and planetary Transits space mission, launched on 2006 December 27, was developed and is operated by the CNES, with participation of the Science Programs of ESA, ESAs RSSD, Austria, Belgium, Brazil, Germany and Spain.

a parameter estimation problem without preference for any specific model. Our method evaluates the *evidence* for the presence of each one of a given number of Lorentzian profiles. This allows us to deal with detection and non-detection of p modes in a power spectrum. It improves the parameter determination for clearly present signal by reducing the negative effects of over-fitting.

2. The probability of a p-mode power spectrum model

In the following subsection we present a very brief introduction in Bayesian formalisms, including the likelihood function, and the definition and role of priors as prerequisites for explaining our approach to determine pulsation frequency spectra and their characteristic parameters from noisy data.

First, although the properties of solar-type oscillations have been well presented by others (see e.g., Appourchaux et al. 1998), a brief summary is necessary before describing our technique. From the equation of a damped harmonic oscillator forced by a random function, the average power of the Fourier transform of the displacement vector can be approximated as,

$$\langle P(\omega) \rangle \simeq \frac{1}{4\omega_0^2} \frac{\langle P_f(\omega) \rangle}{(\omega - \omega_0)^2 + \gamma^2}, \quad (1)$$

where P_f is the power of the Fourier transform of the forcing function, and ω_0 and γ are the angular mode frequency and the damping term, respectively. If the spectrum of the forcing function only slowly varies with the frequency, the resulting average p-mode profile can be approximated by a Lorentzian profile as

$$P(f, \nu, h, \tau) = \frac{h}{1 + 4(f - \nu)^2 / \eta(\tau)^2}, \quad (2)$$

where ν is the mode frequency, f is some frequency value in the spectrum, and h and η are the height and width ($\eta(\tau) = (\pi\tau)^{-1}$, with τ being the mode lifetime) of the profile in the power density spectrum, respectively. For non-radial modes ($\ell > 0$) stellar rotation can lead to the observation of rotational splitting. This can be modeled by adding 2ℓ Lorentzian profiles, spaced with integer multiples of the rotation frequency around the central mode. In this case, Equ. 2 is replaced by

$$P(f, \nu, \nu_{\text{rot}}, h, \tau) = \sum_{m=-\ell}^{\ell} \frac{h_m}{1 + 4(f - \nu + m\nu_{\text{rot}})^2 / \eta(\tau)^2}, \quad (3)$$

where ν_{rot} is the rotational splitting. The mode heights h_m of the additional profiles with $m \neq 0$ are determined by the observed geometry, respectively the inclination angle. In general, the mode height is connected to the mode amplitude (often called the rms amplitude because it corresponds to the rms scatter the mode generates in the time series) according to $a^2 = \pi\eta h$. The power spectrum of observed solar-type p modes typically shows such profiles and usually a Maximum Likelihood Estimation (MLE) algorithm is used to find a best fit between the observed power spectrum and a model like

$$P_m(f) = b + \sum_i P(f, \nu_i, h_i, \tau_i),$$

with b being the background noise (which is assumed to be locally white) and $P(f, \nu_i, h_i, \tau_i)$ being the power of the individual profiles at some frequency (ν -bin) f .

2.1. Application of Bayes theorem

Bayesian logical data analysis frames a problem in terms of an equivalent to Bayes' theorem given by

$$p(A|D, I) = \frac{p(A|I)p(D|A, I)}{p(D|I)}, \quad (4)$$

where $p(A|D, I)$ is the probability for some hypothesis A given the data D and the prior information I . This is also called the posterior probability of A . $p(A|I)$ is the so-called prior probability of A , $p(D|A, I)$ is called the likelihood function, and $p(D|I)$ is the global likelihood. The latter serves as a normalising constant and ensures the total probability over all hypotheses being 1. An extensive introduction to this field and the relevant methods can be found in Gregory (2005).

The necessary task for creating a Bayesian formulation for any problem consists of identifying and assigning probabilities for the individual terms in Equ. 4. The probability of these terms in case of model fitting to observed data is discussed in the following section.

2.2. The likelihood function

The distribution of a number of realisations in the power spectrum of a single solar-type oscillation around its mean Lorentzian profile is given by a χ^2 distribution with two degrees of freedom. Thus, when comparing a model Lorentzian profile to observed data, the probability for the model spectrum m – in the absence of noise – is given by

$$p(m) = \prod_f \frac{1}{P_m(f)} e^{-(P_o(f)/P_m(f))}, \quad (5)$$

where $P_o(f)$ is the observed power at frequency f , and $P_m(f)$ denotes the corresponding power given by the model. Equ. 5 therefore is an appropriate *likelihood function*. It is also used in the MLE method, but the Bayesian formalism contains additional prior probabilities for each of the parameters from which the model spectra are constructed. Equ. 5 has already been suggested for a Bayesian treatment of solar-type oscillations (Appourchaux 2008; Benomar 2008). However, we disagree with the authors opinion that the prior probability should have a negligible influence on the posterior probability. If the posterior probability were to be only weakly influenced by the priors, no information about the noise in the spectrum, except for its overall distribution about the mean noise level given by a χ^2 distribution with 2 d.o.f., could be considered in the calculation of probabilities.

To illustrate our argument, Equ. 5 could be extended by including a factor $p(f)$, denoting the probability for a signal at frequency f not being due to noise, so that

$$p(m) = \prod_f \frac{1}{P_m(f)} e^{-(P_o(f)/P_m(f))} p(f). \quad (6)$$

These probabilities can be evaluated for instance using SigSpec (Reegen 2007). The inclusion of the frequency probabilities with respect to noise, however, only results in an additional factor which cancel out in the comparison of different parameter values and even of different models, since it appears in the numerator as well as in the denominator of Equ. 4. This lack of information about the confidence in specific features in the power spectrum can lead to over-fitting at low signal-to-noise ratios (SNRs). Noisy regions, or even particular peaks, can in principle be represented by Lorentzian profiles over-imposed on the mean noise

level. A model containing these additional profiles on top of the noise level can lead to a higher value of the likelihood function compared to a model that only consists of a constant offset in power. Consequently, a higher value of the likelihood function does not necessarily imply the presence of a Lorentzian profile caused by solar-type pulsation. Therefore, prior probabilities are needed if one wants to include any measure of evidence for the actual presence of p-mode profiles in the posterior probability.

2.3. The role of the priors - improving the MLE approach

The priors should incorporate already obtained information (e.g., parameter uncertainties from other observations). In the case of no prior observations, some problems might be tackled by using theoretical predictions for these terms. In the case of solar-type oscillations, however, models still struggle to accurately reproduce the measurements even for the Sun. We therefore think that when it comes to fitting Lorentzian profiles, ignorance priors (or *uninformative priors*) should be used. First, these have the main purpose of formulating the (lack of) knowledge about specific model properties. Second, they also serve as constraints for boundary values (e.g., upper and lower limits for frequency parameters) in a probabilistically correct way. Third, ignorance priors can be designed to put certain constraints on the posterior probabilities with respect to the likelihood function with the goal that higher probabilities from the likelihood function are necessary towards more questionable parameter values in order to outweigh the bias due to the prior. Using such priors, for example, can provide conservative constraints for signal power in the presence of noise.

The simplest model of a p-mode profile consists of four parameters: mode frequency, mode height, mode lifetime, and background offset. Physically, the mode height and mode lifetime parameters are correlated. However, here we refrain from using this information and assume them to be independent. This enables us to use the mode height parameter as a device to distinguish between a detection and a non-detection of p-mode signal. Our suggestions, with respect to the assignment of ignorance priors, are as follows.

1. Mode frequency ν , mode lifetime τ , background offset b : uniform prior of the form

$$p(x|I) = \frac{1}{x_{\max} - x_{\min}}, \quad (7)$$

where x stands for the respective parameters. For the prior of the frequency parameter this is an appropriate choice, since we cannot *a priori* exclude for an observed spectrum any value within the range defined by the upper and lower p-mode frequencies. One could use the probabilities for each frequency bin mentioned in Sec. 2.2 to include information to the frequency prior about the uncertainties of the observed data. However, the main constraint for the marginal distribution of the central frequency parameter of the Lorentzian profile is the χ^2 distribution around the mean Lorentzian profile, rather than the noise. Therefore, the likelihood function should take care of the frequency determination. The mode lifetime and the background offset, as long as they do not vary across the fitted part of the spectrum by more than a magnitude, are mostly determined by the global properties of the power spectrum and therefore also warrant a uniform prior.

2. Mode height h : modified Jeffrey's prior of the form

$$p(h|I) = \frac{1}{k_h(h + h'_{\min})}, \quad (8)$$

where

$$k_h = \log \left(\frac{h'_{\min} + h_{\max}}{h'_{\min}} \right), \quad (9)$$

and h'_{\min} denotes a value > 0 expressing the “strength” of the prior. The lower h'_{\min} the less probable is a value of h_{\max} . In contrast to the uniform prior, the Jeffrey's prior is normally employed to ensure a uniform probability density per decade (e.g., the prior probability of a value between 0.001 and 0.01 is the same as for a value between 0.01 and 0.1). The modified prior behaves just like a Jeffrey's prior for $h > h'_{\min}$, yet allows for values smaller than h'_{\min} . In this regime it acts like a standard uniform prior and avoids a logarithm of 0.

Any evidence for significant power at some frequency f can be handled with such a combination of priors, if in the Bayesian framework is restricted to ignorance priors. The modified Jeffrey's prior of the mode height provides a solution for the problem that in real observations power due to noise might be mistaken for actual intrinsic signal. Only if the likelihood function delivers significantly higher probabilities for mode heights well above the noise level, it neutralises the mode height prior's preference for a non-detection. The choice of h'_{\min} in this context is therefore nothing more than the expression of an “odds ratio condition”. The posterior probability of the mode height at some value h , without considering the additional parameters, is

$$p(h|D, I) \propto p(h|I)p(D|h, I). \quad (10)$$

The ratio of the probabilities

$$O_{h, h'_{\min}} = \frac{p(h|I)}{p(h'_{\min}|I)} \frac{p(D|h, I)}{p(D|h'_{\min}, I)} = O_{\text{prior}} \times O_{\text{likelihood}} \quad (11)$$

is an odds ratio for the models “mode height = h ” and “mode height = h'_{\min} ”. It can also be seen as a Bayesian weighting of a likelihood ratio, or as a strength-of-evidence indicator similar to a SNR. O_{prior} is the prior odds ratio, while $O_{\text{likelihood}}$ is often called the “Bayes factor”.

$$O_{\text{cond}} = \frac{1}{O_{\text{prior}}} < O_{\text{likelihood}}, \quad (12)$$

accordingly, is then an “odds ratio condition” for the definite detection of the Lorentzian profile. If O_{cond} is larger than $O_{\text{likelihood}}$, the model “mode height = h'_{\min} ” is favoured, and there is not enough evidence for the detection of the corresponding Lorentzian profile. $O_{\text{cond}} = 10^5$, e.g., requires a likelihood function value of a given h which is at least 10^5 times that of h'_{\min} in order to consider a profile as detected. That this condition arises for the mode height parameter is quite intuitive, since the mode height is the parameter that determines whether a Lorentzian profile rises above the noise level. In addition, the mode height clearly is a scale parameter, rather than a location parameter (see Gregory 2005), which also points at a Jeffrey's prior as the obvious choice. Choosing h'_{\min} allows to set a lower limit for the required definite detection. The MLE procedure does not implicitly allow for such a restriction, as the evaluation of the fitting function crucially depends on the white noise properties of the spectrum, which makes the MLE procedure prone to overfitting.

In the more complicated case of rotationally split modes, these priors also allow us to refrain from any preceding mode identification, which is usually necessary because modes of different spherical degree have different shapes due to their 2ℓ split components. If rotational splitting is suspected, one simply replaces single Lorentzian profiles with a sum of profiles. The central Lorentzian of the rotationally split mode can be treated just like a single profile, i.e., it has the same parameters and corresponding priors. The suspected split components, however, are simply characterized by their mode heights and the stellar rotation frequency (see Equ. 3). Thus, the same type of mode height and frequency priors can also be applied to these additional parameters. Again, the height prior only allows significant mode heights of those profiles in the rotationally split multiplet for which there is enough evidence in the data.

2.4. The posterior probability

Combining the previously explained terms results in the expression for the posterior probability of a combination of parameter values

$$p(v, h, \tau, b|D, I) \propto \left(\prod_{x=v, h, \tau, b} p(x|I) \right) p(D|v, h, \tau, b, I) = \left[\left(\prod_{x=v, \tau, b} \frac{1}{x_{\max} - x_{\min}} \right) \frac{1}{k_h(h + h'_{\min})} \right] \times \prod_f \frac{1}{P_m(f)} e^{-(P_o(f)/P_m(f))}, \quad (13)$$

where the product over x denotes the product of the individual prior probabilities of each parameter. The term in the square brackets is thus the combined prior probability, while the last term, see Equ. 5, is the likelihood function. In the case of n Lorentzian profiles fitted to the same data, this equation becomes

$$p(v_{1..n}, h_{1..n}, \tau_{1..n}, b_{1..n}|D, I) \propto \left[\prod_{i=1}^n \left(\prod_{x=v_i, \tau_i, b_i} \frac{1}{x_{\max} - x_{\min}} \right) \frac{1}{k_h(h_i + h'_{\min})} \right] \times \prod_f \frac{1}{P_m(f)} e^{-(P_o(f)/P_m(f))}. \quad (14)$$

Depending on the fitted model and additional assumptions, Equ. 14 can be simplified by considering a single background offset for all profiles instead of n . If one does not suspect the mode lifetime to vary among each profile by large amounts, the number of parameters can be further reduced by $n-1$.

Equation 14 causes a problem when a large number of Lorentzian profiles are fitted to noisy data. The combined modified Jeffrey's priors would become too strong. Even if clear p-mode signal is present, the likelihood function would not be able to neutralise the priors. Consequently, not all Lorentzian profiles in the power spectrum could be recognised. In the simplest case the problem can be averted by employing regional, rather than global fitting. However, any parameters that are constant across the spectrum will be less accurately constrained. Another (rather heuristic) possibility to handle this situation is to systematically increase h'_{\min} with the number of Lorentzian profiles, which is equivalent to lowering the odds ratio condition in terms of Equ. 11.

A better approach is to exchange the product of mode height priors in Equ. 14 with its geometric mean. This is equivalent to modifying the prior probability for the mode height so that

$$p_n(h|I) = \left[\frac{1}{k_h(h + h'_{\min})} \right]^{1/n}, \quad (15)$$

where n is the number of Lorentzian profiles (including rotationally split components) in the model. The geometric mean ensures that the mode height prior can be interpreted as in Equ. 11, but for the whole fitted spectrum. The resulting odds ratio becomes

$$O_{h_1, \dots, h_n; h'_{1, \min}, \dots, h'_{n, \min}} = \left(\prod_{i=1}^n \frac{p_n(h_i|I)}{p_n(h'_{i, \min}|I)} \right) \frac{p(D|h_1, \dots, h_n, I)}{p(D|h'_{1, \min}, \dots, h'_{n, \min}, I)} = \frac{\langle p(h_i|I) \rangle}{p(h'_{\min}|I)} \frac{p(D|h_1, \dots, h_n, I)}{p(D|h'_{1, \min}, \dots, h'_{n, \min}, I)} = O_{\text{prior}} \times O_{\text{likelihood}}. \quad (16)$$

This odds ratio is then a general property of the model spectrum, independent of the number of mode height parameters. It is a comparison of a model with mode heights of h_1, h_2, \dots, h_n , to a model where all $h_i \leq h'_{\min}$ (i. e., the power spectrum is consistent with noise). The corresponding odds ratio condition is the same as in Equ. 12. An example for the importance of parameter h'_{\min} is discussed in Sec. 4. For all analyses reported in this paper, we use Equ. 15 unless mentioned otherwise.

The probabilities of different models with different numbers of parameters can be easily compared with Bayesian probabilities. This is because Bayes' theorem formally contains the principle of "Occam's razor": when two models are able to explain data equally well, the one with the smaller number of new assumptions (= model parameters) is to be favoured. Taking the geometric mean of the mode height prior will not break this principle when models of p-mode spectra of different complexity are compared. Only when the odds ratio derived from a given h'_{\min} is in favour of additional profiles with $h \gg h'_{\min}$, these can warrant a value larger than h'_{\min} . Additional Lorentzian profiles with $h \sim h'_{\min}$, however, are equivalent to non-detections. As such, they can be removed from the model.

3. Application using Markov-Chain Monte Carlo

The analytic evaluation of complex models in a large parameter space in terms of Bayesian probability soon reaches the limit of computer resources. Stochastic methods can provide a sufficient sampling of the parameter regions of interest at a much smaller cost. In particular applications of the MCMC-technique have therefore gained momentum and the (Bayesian) problems to which MCMC nowadays are applied range from the detection of planets (Gregory 2007), to the analysis of solar-type pulsators (Brewer et al. 2007), to spot modelling of active stellar atmospheres (Croll 2006).

Basically, MCMC performs a biased random walk through the parameter space of a specific problem. Each parameter is incremented or decremented by some random fraction of a predefined step width and the procedure then accepts or declines this combination of steps. The condition of acceptance is provided by the *Metropolis-Hastings* algorithm, which is based on the ratio of probabilities of subsequent parameter configurations before and after the step. In order to comply with this algorithm, the random steps have to be sampled from a symmetric proposal distribution (uniform, Gaussian, etc.). MCMC scales with an increasing number of parameters and it is an ideal tool for solving our problem, which is evaluating the probability of a power

spectrum containing many modes. In addition, the *Metropolis-Hastings* algorithm evaluates only the *relative* probability between different parameter configurations. Thus, the normalisation factor of Equ. 4, which is often very difficult to evaluate and has been neglected throughout this paper when deriving the Bayesian terms, does not need to be calculated.

3.1. Semi-automated MCMC calibration

The most crucial prerequisite of a MCMC-implementation is the calibration of the acceptance rate of subsequent steps. For more than two parameters it has been shown that the acceptance rate should be about 0.25 in order to minimise correlations between the different parameters (Roberts et al. 1997). As the acceptance rate mostly depends on the step width of each parameter these step widths have to be calibrated. A manual calibration becomes more and more inefficient in the case of many parameters and we therefore implemented the following automated MCMC calibration, similar to what is described in Gregory (2005).

Given an observed power spectrum, several non-overlapping frequency windows are defined to constrain the range of the individual mode frequency parameters. The number of Lorentzian profiles to be investigated per window is chosen, and lower and upper constraints for the mode height(s), the mode lifetime(s) and the background offset(s) are defined. The model spectrum is initialised with appropriate starting parameters (e.g., equidistant frequencies within the frequency windows, mean values of the mode height, mode lifetime, and background offset), and the MCMC algorithm is started with a step width of

$$\sigma(x) = 0.1(x_{max} - x_{min}) \quad (17)$$

for each model parameter x , where x_{max} and x_{min} are the upper and lower limits already used to define the prior probabilities. In this so-called “burn-in” phase the MCMC approaches in some hundreds to thousands of iterations the parameter regions of maximum likelihood. This is achieved by evaluating after every single step in every single parameter the relative probability of the models according to Equ. 14, with the option to consider the mode height prior according to Equ. 15. After the “burn-in” phase the model is already close to the global maximum of probabilities, in contrast to more complex problems like spot modelling. For another few thousand of iterations, the *individual* acceptance rate for each parameter is evaluated every few 100 steps. Simultaneously, the MCMC step width of the respective parameter is slowly adjusted to approach a desired acceptance rate which depends on the total number of parameters in the model. For instance, we found that in order to achieve a *combined* acceptance rate of about 0.25 for a model consisting of ~ 70 parameters, *individual* acceptance rates are required to be roughly 0.94.

Once the desired individual acceptance rates remain fairly stable, our algorithm switches to the standard MCMC routine. The probability of a new configuration, and therefore the probability of its acceptance, is evaluated after all parameters have been slightly changed according to a random walk. The MCMC begins now to test automatically the parameter space.

3.2. Evaluating the MCMC results

Since the acceptance probability for each step is calculated using the Bayesian posterior probability, the MCMC will produce correct distributions for each involved parameter. After a sufficient number of iterations the “marginal distributions” for all model

frequencies, mode heights, mode lifetimes, and background offsets can be approximated by interpreting histograms as probability density functions of how frequently respective values of each parameter were visited. An estimate for the validity of the tested model can be obtained by examining these distributions. Sometimes strong asymmetries, multiple local maxima, and other obviously non-Gaussian features hint at how to improve the model. In any case, uncertainties for all parameters can be derived by evaluating the cumulative distribution function of the normalised histograms.

4. Simulations

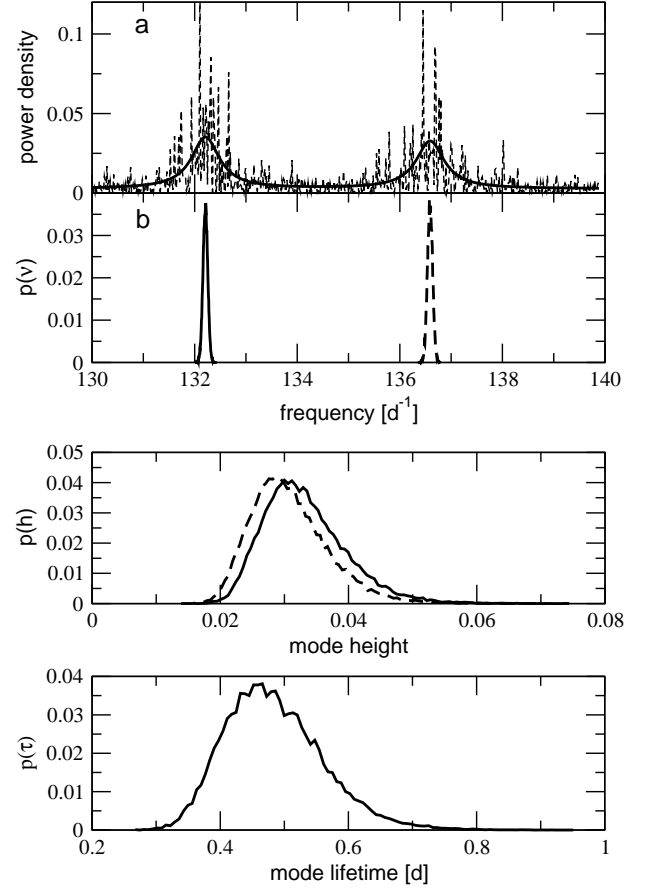


Fig. 1. Results of the Bayesian analysis for one of the 100 simulated data sets. *Upper panel:* (a) the power density spectrum calculated from the simulated data (dashed line) and the most probable model spectrum derived from the analysis (solid line); (b) the marginal distributions of the mode frequency parameters for both Lorentzian profiles of the model. *Middle panel:* the corresponding marginal distributions of the mode height parameters. Dashed and solid lines refer to the respective distributions presented in the top panel (b). *Bottom panel:* the marginal distribution of the mode lifetime parameter.

In order to test our method with parameters similar to a typical CoRoT run (actually the Initial Run) we generated 100 time series of 60 days. Each simulated data set represents a different realisation of the signal described in Tab. 1. The simulation followed the procedure given in Chaplin et al. (1997). We calculated the power spectra of each time series and applied our Bayesian analysis, which was limited to frequencies between

Table 1. Input parameters for the simulated solar-type pulsator.

	f_1	f_2
frequency	132.3	136.6
rms amplitude	1	1
estimated mode height	0.033	0.033
mode lifetime	0.5 d	0.5 d
white noise model with SNR of 0.1 in the time domain		

130 and 140 d^{-1} and based on 300000 iterations of the MCMC. Two Lorentzian profiles were fitted, each with adjustable mode height but equal mode lifetime. The upper and lower limits for all parameters, which also enter the Bayesian formalism via the prior probabilities, are presented in Tab. 2. h'_{\min} was set to 10^{-6} ,

Table 2. Parameter limits for the analysis of the simulated solar-type pulsator. According to Equ. 16, h'_{\min} was set to 10^{-6} .

	<i>min</i>	<i>max</i>
$\nu [\text{d}^{-1}]$	130	140
h	0	0.15
$\tau [\text{d}^{-1}]$	0.1	1.5
b	0.001	0.01

and h_{\max} to 0.15. This corresponds to an odds ratio condition of $\sim 10^5$ for the maximum value h_{\max} and to a condition of $\sim 10^4$ for the actual input mode heights.

4.1. Evaluation of the simulations

Fig. 1 shows a power spectrum calculated from one of the 100 test data sets, as well as the most probable fit to the data. All input parameter values are reproduced in our tests within the borders of the derived marginal distributions. There have been discussions on how to determine appropriate values from the marginal distributions in terms of numbers representing their general properties (see Gregory 2005). We present the median values for all parameters. In any case, the important quantity for comparing observations to models (e.g., mode frequencies) are the uncertainties – not a single value denoted as “best fit” or “most probable”. A closer inspection of Fig. 1 reveals that in the presented case the parameter values derived from the simulated data are not always within the 1σ uncertainties. All parameters are underestimated: The median of the f_1 distribution deviates from the input value by 2.99σ . The corresponding mode height is underestimated by 0.37σ . f_2 is underestimated by 0.63σ , with the corresponding mode height deviating by 1.2σ . The mode lifetime also deviates by 0.84σ . Such deviations can be expected due to the stochastic nature of the signal.

Fig. 2 shows the results for all 100 simulations. The median values derived from our analysis are compared to the simulation input values and are plotted against the corresponding normalised probabilities of these input values, evaluated via the marginal distributions. As expected, the input values are not always reproduced to within 1σ ($p > 0.682$), but are consistently found within 3σ . The scatter of the derived median values of the parameters around the input values behave as expected. The frequency parameter median is shown to be distributed symmetrically, while the mode lifetime and mode heights follow a log-normal distribution. The figure also illustrates the overall accuracy with which each parameter can be reproduced. The fre-

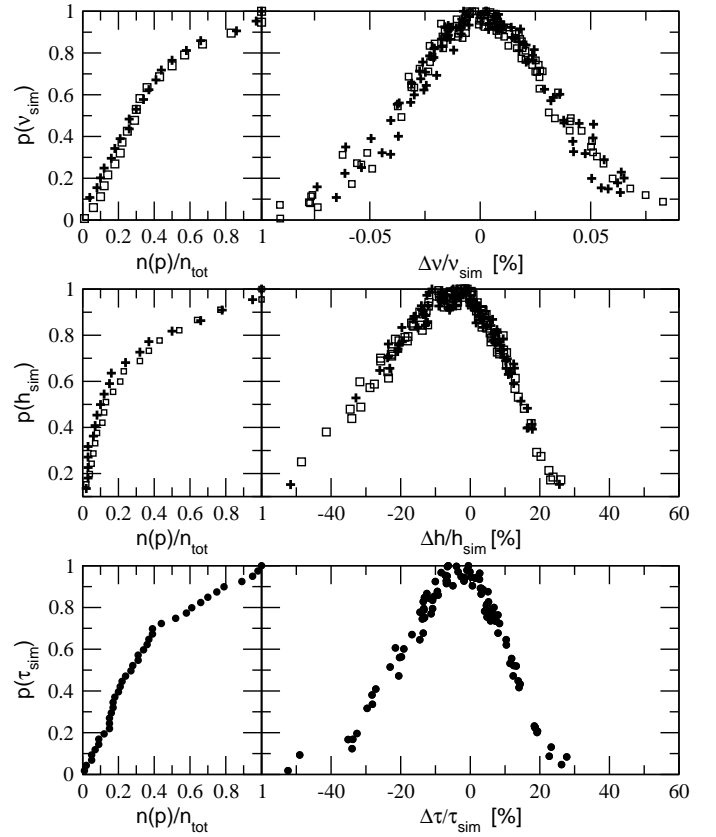


Fig. 2. *Right panels:* distribution of the derived median mode parameter values (ν, h, τ) compared to the input values. Positive/negative values indicate under-/overestimation of the parameters. The open squares and plus signs in the top and middle panels identify the results for the two Lorentzian profiles in the model. *Left panels:* cumulative histograms for the probabilities of the simulation input values determined from all 100 simulations.

quency parameter shows a lower accuracy limit of about 0.1%. The corresponding lower limits for the mode height and mode lifetime parameters are much larger with about 40%. Lastly, Fig. 2 shows cumulative histograms for the parameter value probabilities of the evaluated simulations. These histograms indicate that the scatter of the probabilities of the input values, for individual realisations, can be roughly approximated by a normal distribution. As the derived marginal distributions for all parameters provide a consistent picture, we argue that the probability densities obtained from a single data-set can be trusted.

4.2. The importance of the mode height prior

As was argued in Sec. 2.3, the mode height prior in its given form allows constraining the complexity of a model. The simulations described in the previous Section provide us with an excellent example for this rationale. Fig. 3 shows one of the simulations that included by chance an additional power excess in the frequency range of consideration due to noise and/or the stochastic nature of the input signal. Using this data we tested how the detection of a (non-existent) third Lorentzian profile would be influenced by the h'_{\min} parameter of the mode height prior. We evaluated the probabilities of 3 Lorentzian profiles in the spectrum and performed the analysis with two different values of $h'_{\min} = 10^{-8}$ and $h'_{\min} = 0.01$. The weaker prior with $h'_{\min} = 0.01$

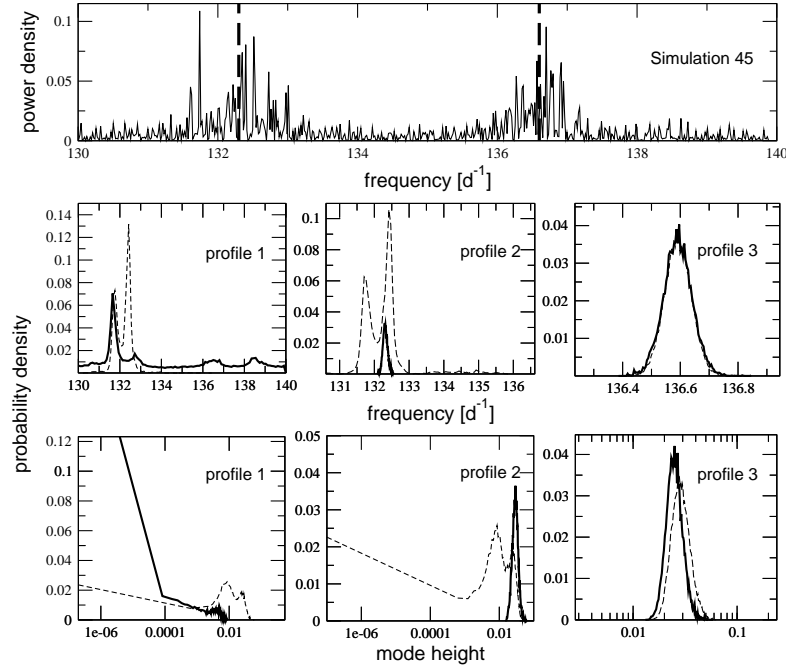


Fig. 3. 3 Lorentzian profiles are fitted to simulated data that contain 2 frequencies. *Top panel:* power density spectrum of one of the 100 simulations mentioned in Sec. 4. The 2 input frequencies are marked by thick dashed lines. Additional power at $\sim 131.7\text{d}^{-1}$ is either due to noise or, more likely, due to the stochastic nature of the signal. *Middle panels:* marginal distributions of the frequency parameters calculated after 300000 iterations. Each panel contains the results for one of the three fitted profiles. The thick lines show the results for $h'_{\min} = 10^{-8}$, the thin dashed lines indicate $h'_{\min} = 0.01$. *Lower panels:* corresponding marginal distributions of the mode height parameters for each of the Lorentzian profiles and for both values of h'_{\min} (10^{-8} and 0.01).

developed a formal lack of self-restriction similar to the MLE method, or other Bayesian methods that do not implicitly treat the problem of over-fitting due to, e.g., noise. The strong prior with $h'_{\min} = 10^{-8}$, however, puts clear constraints on the number of profiles that are considered as definite detections (see Fig. 3).

In the case of the *strong prior*, the marginal distribution of the frequency parameters of profile 2 and profile 3 are good approximations to a normal distribution and match the two input frequencies. Evidently, profile 2 is not influenced by the additional power excess. Profile 1 shows a maximum probability for the frequency parameter at the location of the additional power excess, but the marginal distribution assigns considerable probability densities to the whole parameter range. However, the marginal distributions for the height prior, which again are well-shaped for profile 2 and profile 3, suggest a most probable mode height of zero for profile 1. Therefore, the additional profile is not necessary and only two profiles are clearly detected.

In the case of the *weak prior*, the marginal distributions of the frequency and mode height parameters of profile 1 and profile 2 intersect and mix. Hence, there seems to be evidence for a third Lorentzian profile which is comparably strong to the evidence for the actual Lorentzian profile at 132.3d^{-1} . This third cprofile, however, was not included in the simulation. Moreover, profile 1 and profile 2 cannot be easily separated. Thus, their mode parameters cannot be unambiguously determined. To conclude, in this example there is “evidence” for a non-existent third mode, and the information about the simulated profile is distorted.

5. Application to the CoRoT target HD 49933

We applied our technique to the 60 days of CoRoT N2–data of HD 49933 obtained during the Initial Run from February to March, 2007. A detailed description of the data extraction and reduction can be found in the *CoRoT book* (see Baglin et al. 2006, and references therein). The data set consists of more than 163 000 measurements sampled each 32 s. A detailed summary of the stellar properties and the CoRoT observations is given by Appourchaux et al. (2008).

Intrinsic stellar noise–like signal, mainly due to turbulent convection, generates significant power in the frequency range of pulsation and effects the accurate determination of mode parameters. For the Sun Harvey (1985) modeled the background signal with a sum of power laws. Aigrain et al. (2004), and more recently Michel et al. (2008), use $P(\nu) = \sum_i P_i$, with $P_i = a_i \zeta_i^2 \tau_i / (1 + (2\pi\tau_i\nu)^{C_i})$, or hereafter $P_i = A_i / (1 + (B_i\nu)^{C_i})$, to model the solar granulation signal, where ν is the frequency, τ_i is the characteristic times scale of the i th component and C_i is the slope of the power law. The normalisation factor a_i is chosen such that $\zeta_i^2 = \int P_i(\nu) d\nu$ corresponds to the variance of the stochastic signal in the time series. Whereas the slope of the power laws was arbitrary fixed to 2 in Harvey’s original model, Appourchaux et al. (2002) were the first to suggest a different value. Recently, Aigrain et al. (2004) and Michel et al. (2008) have shown that, at least for the Sun, the slope is closer to 4. Each power law represents a different physical process with time scales for the Sun ranging from minutes in the case of granulation to days in the case of stellar activity.

Appourchaux et al. (2008) used a single power law for the background signal in the frequency range of pulsation and fitted the corresponding parameters simultaneously with the p -mode parameters to the observed power density spectrum. We have

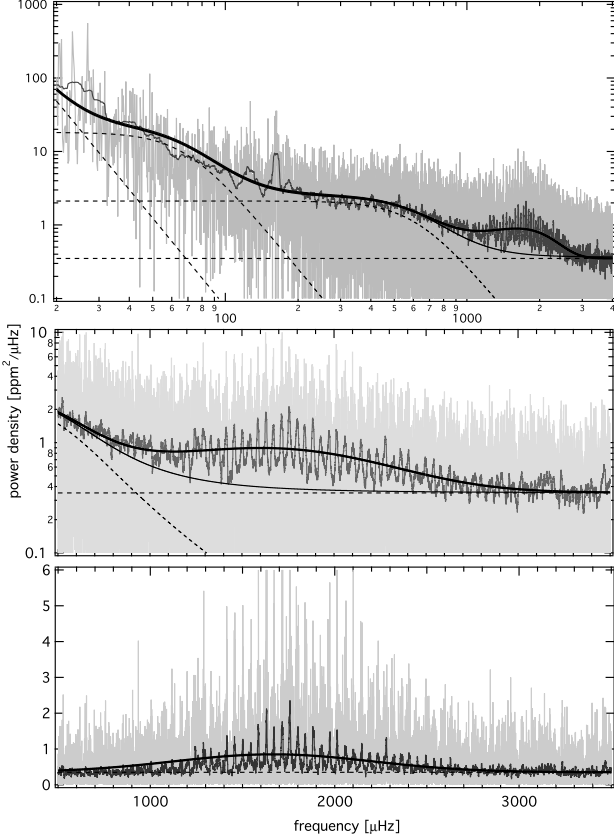


Fig. 4. *Top panel:* power density spectrum of HD 49933. Light grey: original power density spectrum; dark grey: the original spectrum smoothed with a $20\mu\text{Hz}$ boxcar average; thick solid line: global fit according to Equ. 18; dotted line: global fit without the Gaussian term; dashed lines: white noise and the 3 power law components of the global fit. *Middle panel:* enlargement of the top panel. Dotted line: background fit plus the Lorentzian profiles fitted to the residual power density spectrum. *Bottom panel:* original power density spectrum with the granulation signal removed. Solid line: Gaussian term of the global fit.

separated the analysis of the background signal from the analysis of the pulsation signal, in which case one has to model the pulsation signal in the power density spectrum with a dedicated term in the global background fit. Kallinger et al. (2008b) have shown that the power excess hump due to pulsation can be approximated by a Gaussian function. Hence, our global model to fit the heavily smoothed power density spectrum of HD 49933 consists of a superposition of white noise, three power law components, and a power excess hump approximated by a Gaussian function:

$$P(\nu) = P_n + \sum_{i=1}^3 \frac{A_i}{1 + (B_i \nu)^4} + P_g \cdot e^{-(\nu - \nu_{\max})^2 / (2\sigma^2)}, \quad (18)$$

where P_n is the white noise component, A_i and B_i are the amplitudes and characteristic time scales of the power laws, P_g , ν_{\max} , and σ are the height, central frequency, and width, respectively, of the Gaussian term. The resulting global fit (and its components) is shown in the top and middle panel of Fig. 4 along with the original and heavily smoothed power density spectrum. The corresponding parameters of the global fit are given in Tab. 3.

Table 3. Global fit parameters. The amplitudes of the power laws (A_i), the height of the Gaussian part (P_g), and the white noise components (P_n) are given in $\text{ppm}^2/\mu\text{Hz}$. The power law time scales (B_i) are given in seconds and the center (ν_{\max}) and width (σ) of the Gaussian part are in μHz . One-sigma error estimates are given in brackets.

	A_1 B_1	A_2 B_2	A_3 B_3
Power laws	25743 (6200) 252311 (25000)	22 (6) 16477 (1950)	2.2 (0.11) 1637 (62)
	P_g	ν_{\max}	σ
Gaussian term	0.500 (0.015)	1657 (28)	538 (26)
White noise	$P_n = 0.33$ (0.005)		

The fit without the Gaussian component (dotted line in top and middle panel of Fig. 4) enables us to estimate the local noise and is used to separate the background signal from the pulsation signal. The residual power density spectrum rescaled to the white noise level, shown in the bottom panel of Fig. 4, is used for the subsequent analysis.

5.1. MCMC analysis

The frequency range between the lower and upper limits beyond which we see the pulsation signal disappearing in the noise was subdivided into 16 windows. To each, a chosen number of Lorentzian profiles was fitted, based on our Bayesian algorithm. The model parameters are presented in Tab. 4. This subdivision into windows was only chosen to accelerate the burn-in phase. It has no influence on the results, as long as the resulting marginal distributions for the mode frequency parameters are not intersected by the window borders. Yet, it still enables us to perform a global fit which includes the influence of Lorentzian profiles also from adjacent windows.

Table 4. Parameter limits for the analysis of HD49933. The height prior parameter was set to $h'_{\min} = 10^{-8}$.

	<i>min</i>	<i>max</i>
$\nu [\mu\text{Hz}]$	1219.9	2618.1
$h [\text{ppm}^2/\mu\text{Hz}]$	0	6
$\tau [\text{d}^{-1}]$	0	1.5
$b [\text{ppm}^2/\mu\text{Hz}]$	0.001	0.5

For the first analysis we decided to consider only 2 Lorentzian profiles in each window. Moreover, we also kept the mode lifetime uniform for all Lorentzian profiles, expecting that the marginal distribution of this parameter would tell us whether this assumption is valid.

Fig. 5 shows the power density spectrum, on which our analysis is based, together with the fitting windows we defined, and the most probable model derived after ~ 1.3 million iterations. The model manages to reproduce the observations quite well, and there remain only very few frequency ranges where a visual inspection seems to indicate additional power. Beyond $\nu > 2450\mu\text{Hz}$ several Lorentzian profiles are fitted with fairly well defined frequencies, but with a probability maximum for a

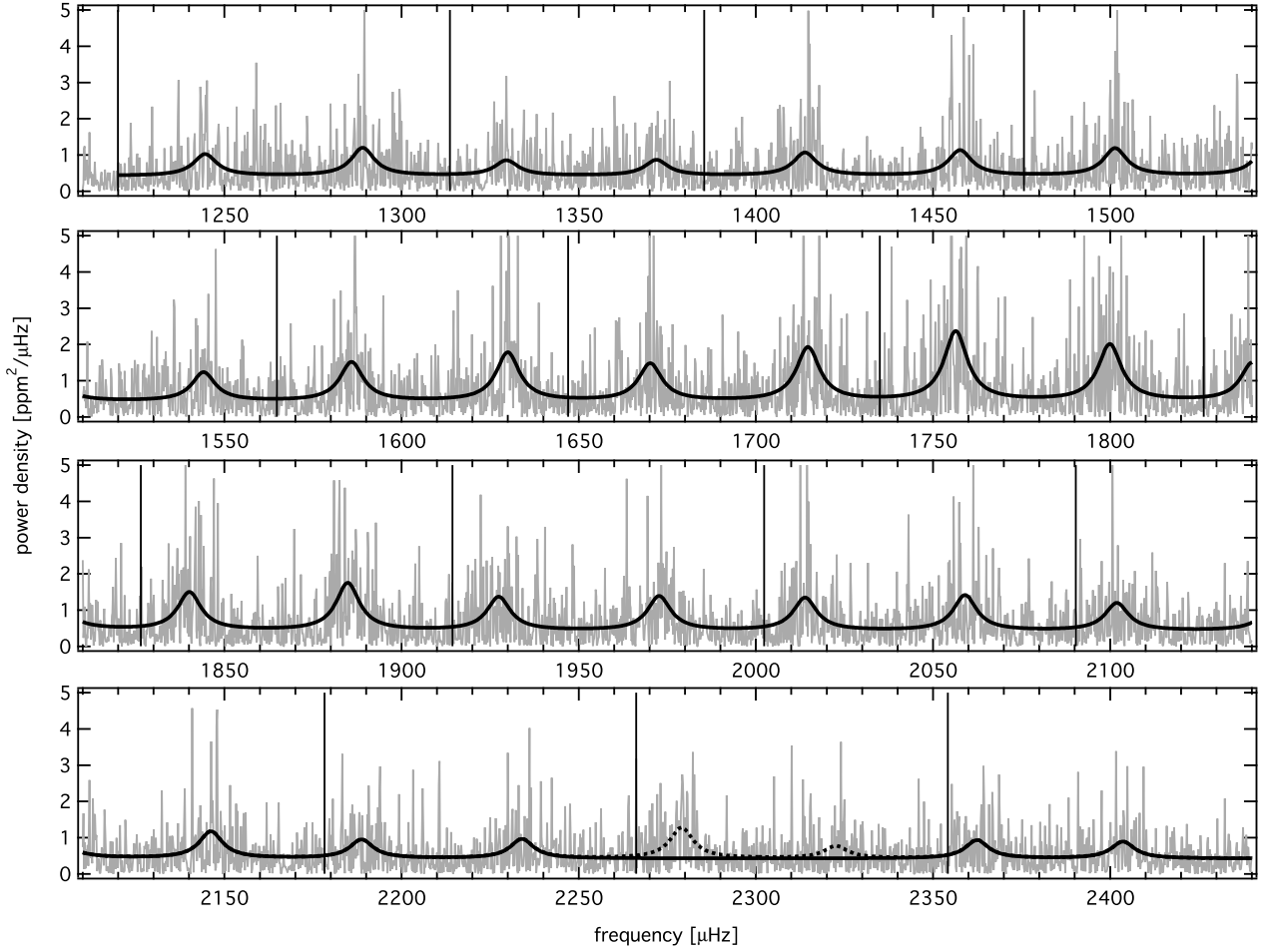


Fig. 5. Observed power density spectrum (gray) and fitted Lorentzian profiles. Vertical lines indicate the borders of the fitting windows (see text). The dashed lines in the bottom panel show two profiles for which our Bayesian technique results in ambiguous frequency distributions ranging over the whole fitting window

mode height of zero. Two profiles, listed in Tab. 5 as P25 and P26, indicated in the figure by dashed lines, have ambiguous frequency distributions ranging over the whole fitting window. What is shown is a biased choice to fit the general picture.

Fig. 6 presents an example for the marginal frequency distribution and mode height for one of the Lorentzian profiles. The bottom panel shows a quite narrow and smooth mode height distribution for a simultaneous fit to all Lorentzian profiles, indicating a constant mode lifetime. The data therefore do not seem to warrant different mode lifetimes. It is thus safe to assume that any variations among the various profiles for this parameter are accounted for within the uncertainty given by the mode lifetime distribution. Surprisingly, we do not find well-defined multi-modal distributions for any of the frequency parameters involved. Some ambiguities in the distributions are only apparent at very high frequencies and with the poorest SNR. Additional profiles, either due to modes of higher degree or rotational splitting, still could be present, if the frequencies are very well separated.

5.2. On the evidence for $\ell = 2$ modes

To decide on this serious problem, we first tested the claim by Appourchaux et al. (2008) who reported the detection of $\ell = 2$ modes and repeated our analysis for the region with the high-

est SNR, but included for each fitting window a third Lorentzian profile in our model. The results are shown in presented in Fig. 7. The probability distributions for the additional profiles consistently favours a mode height of zero. Moreover, the corresponding mode frequency distributions only vaguely contain regions of higher probability, and even these regions frequently cannot be reconciled with the frequency values given in Appourchaux et al. (2008). We therefore conclude that, based on our conservative approach, any additional power in the power density spectrum is due to noise or to the stochastic nature of the clearly detected modes. From our perspective, the data do not present convincing evidence for $\ell = 2$ modes.

5.3. On the evidence for rotational splitting

The failed detection of additional profiles, and the single-mode nature of the frequency distributions of detected profiles, suggests that the effects expected from rotational splitting can most likely be neglected in the analysis of the CoRoT data of HD 49933. Nonetheless, in order to perform a more rigorous test, we analysed the same frequency region shown in Fig. 7 including these effects. Our model used 2 Lorentzian profiles per fitting window, each of which contains 2 additional features corresponding to rotational splitting of $\ell = 1$ modes (see Equ. 3). Accordingly, a new global parameter, the rotation frequency, was

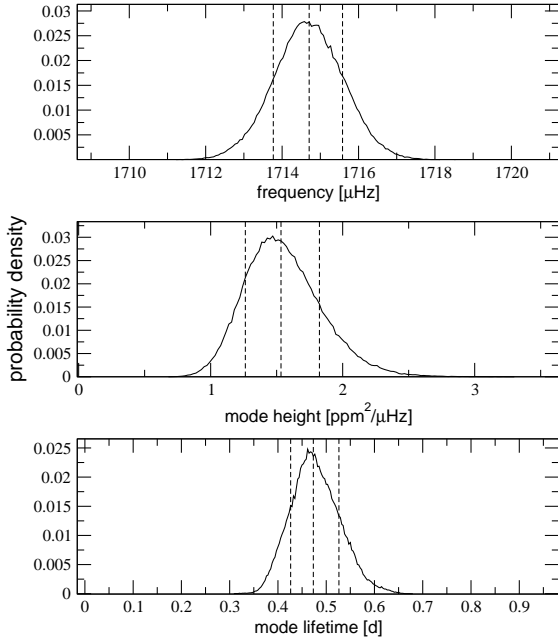


Fig. 6. *Top panel:* marginal distribution of the mode frequency parameter of one of the profiles fitted to the CoRoT data. The median value, and the lower and upper 1σ -values are indicated by the dashed lines. *Middle panel:* same as top panel but for the corresponding mode height parameter. *Bottom panel:* same as top panel but for the mode lifetime parameter for a simultaneous fit to all Lorentzian profiles.

introduced. Appourchaux et al. (2008) report the detection of a particular spectral feature at $3.4 \mu\text{Hz}$ which apparently corresponds to the HD 49933's rotation frequency. We therefore used this value as a reference and allowed a scatter of about $0.2 \mu\text{Hz}$ in either direction. This range corresponds to twice the frequency resolution $(\Delta T)^{-1}$ of the CoRoT time series, where ΔT is the length of the data set, and was used to define the borders of a uniform prior. The heights of the rotation profiles were implemented as usual, using modified Jeffrey's priors for these parameters. We expected a well defined distribution for the rotation frequency to emerge from the analysis, provided that the claim of Appourchaux et al. (2008) was correct. However, we find no preferred value for this parameter, as is shown in Fig. 8. The distribution is mostly consistent with sampling noise. Concerning the mode heights, alternating detections and non-detections of the rotation profiles would indicate a difference in their central profiles between radial and non-radial modes. Alas, we cannot find any such differences, since the mode height distributions for the rotation profiles are consistent with a null result. While the star certainly does rotate, it seems that the signal is too close to the noise level to support any need for these parameters. In other words, rotational effects, if present, seem to be ill-defined and do not need to be considered for the frequency analysis of this data set. As an example of an ideal case, the bottom panel of Fig. 8 shows corresponding results from a single mode using 60 days of data of the Sun observed as a star by the VIRGO (green band) instrument on board the SOHO spacecraft (see Fröhlich et al. 1997, and references therein). Fitting only the small range between 3090 and 3110 μHz and using the same profile model as for HD 49933, the rotational splitting becomes apparent.

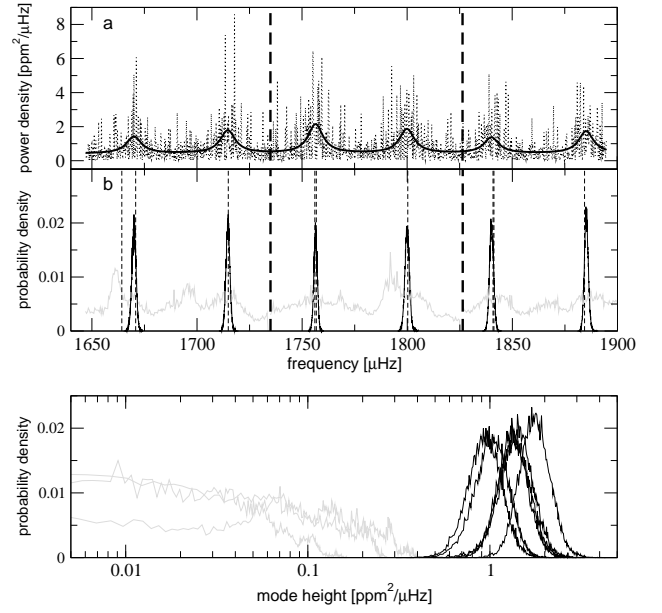


Fig. 7. *Top panel:* (a) the fitted region in the power density spectrum, where the p modes have the highest SNR. The most probable model (thick solid line) is presented in comparison to the observations (dotted line). The borders of the fitting windows are indicated by the thick dashed lines. (b) The marginal mode frequency distributions for 3 profiles per window. Six profiles are identified (black), while the additional profiles are ambiguous across the whole frequency range (gray lines). Frequencies identified by Appourchaux et al. (2008) are shown as thin dashed lines. *Bottom panel:* The corresponding mode height distributions.

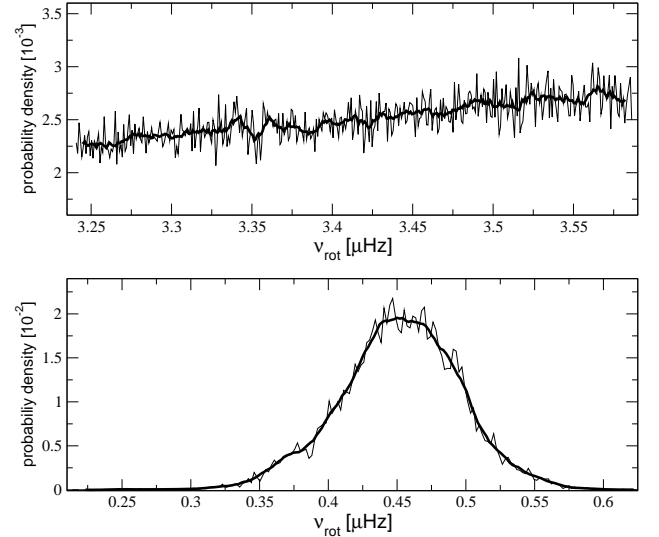


Fig. 8. *Top panel:* the marginal distribution of the rotational splitting parameter derived as explained in Sec. 5.3. The thick black line is a boxcar average using 10 data points. *Bottom panel:* the same but for the analysis of VIRGO data of the Sun.

5.4. Results

Thus, we return to our analysis using only 2 modes per window without any rotational splitting. For 6 of the 32 fitted profiles, the identification is ambiguous (or the most probable mode heights are close to zero) due to the low SNR. All other profiles

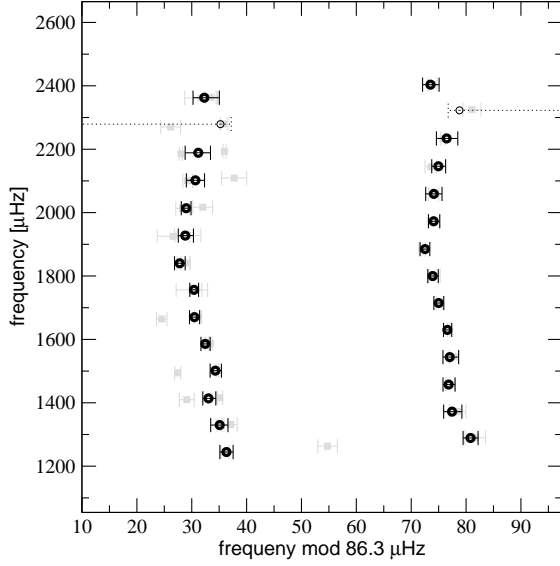


Fig. 9. Echelle diagram showing the identified frequencies (solid error bars). Values belonging to profile 25 and 26 (see Tab. 5) are indicated by the dashed error bars. Frequencies found by Appourchaux et al. (2008) are displayed in grey.

are clearly detected and their parameters have smooth, single-mode distributions. The results of our analysis are presented in Tab. 5. The 1σ -errors have been derived from the cumulative distribution functions, which are evaluated using the marginal distributions for all parameters. We find that the data are consistent with a mode lifetime of roughly 0.5 days which does not appear to vary significantly across the spectrum. The confidence for this overall result can be calculated via the mode height parameter. As we have used $h'_{min} = 10^{-8}$, the result gives an odds ratio condition $O_{cond} = 4.07 \times 10^6$.

Therefore, the obtained parameter distributions are at least 4.07×10^6 times more probable than a model spectrum that only consists of the background offset. The profiles 25 and 26 are only listed for sake of completeness. Due to the ambiguity in their marginal frequency distribution, apparent in their given uncertainties, we do not assign credibility to these values. The final Echelle diagram is displayed in Fig. 9. The frequencies estimated as $\ell = 1$ by Appourchaux et al. (2008) agree very well with our corresponding values, and the 1σ -uncertainties are comparable in both studies. The remaining frequencies, however, differ due to the cited authors' explicit assumption of $\ell = 2$ modes, which we do not detect.

Although we deliberately did not include fixed mode height ratios for modes of different degree in our model, the resulting mode height ratios are mostly consistent within the uncertainties with a fixed ratio, an assumption made by Appourchaux et al. (2008). The obvious outlier in Fig. 10 at $\sim 2280 \mu\text{Hz}$ is due to profiles 25 and 26, which we already marked as highly suspicious.

6. Discussion

We have presented a conservative approach for a Bayesian analysis of solar-type p modes. The method achieves its credibility due to the specific application of the mode height prior as a false-alarm test, and the deliverance of the marginal distributions of all parameters. It was shown that the algorithm reproduces simulations very well and that it helps to constrain the model com-

Table 5. Results of the CoRoT data for HD 49933. Profiles P 25 and P 26 are ambiguous detections. Profiles P 29 to P 32, which are not listed, have a most probable mode height of zero.

P	ν [μHz]	σ_ν	h [ppm ² / μHz]	σ_h
1	1244.53	(-1.21 / +1.21)	0.60	(-0.15 / +0.17)
2	1289.02	(-1.36 / +1.36)	0.81	(-0.19 / +0.19)
3	1329.60	(-1.50 / +1.64)	0.45	(-0.14 / +0.14)
4	1371.94	(-1.80 / +1.53)	0.47	(-0.14 / +0.15)
5	1413.85	(-1.34 / +1.03)	0.67	(-0.15 / +0.17)
6	1457.63	(-1.17 / +1.02)	0.74	(-0.17 / +0.17)
7	1501.40	(-1.11 / +0.95)	0.76	(-0.17 / +0.20)
8	1544.11	(-1.63 / +1.22)	0.83	(-0.19 / +0.20)
9	1585.86	(-0.90 / +0.78)	1.08	(-0.20 / +0.22)
10	1629.99	(-0.81 / +0.70)	1.35	(-0.23 / +0.26)
11	1670.18	(-0.96 / +0.89)	1.08	(-0.22 / +0.23)
12	1714.71	(-0.94 / +0.88)	1.53	(-0.27 / +0.29)
13	1756.42	(-0.82 / +0.76)	2.01	(-0.34 / +0.37)
14	1799.91	(-1.02 / +0.89)	1.61	(-0.28 / +0.32)
15	1840.10	(-1.00 / +0.94)	1.04	(-0.19 / +0.23)
16	1884.81	(-0.89 / +0.89)	1.38	(-0.25 / +0.27)
17	1927.41	(-1.50 / +1.27)	0.93	(-0.20 / +0.23)
18	1972.70	(-1.10 / +0.94)	0.97	(-0.19 / +0.22)
19	2013.88	(-0.89 / +0.89)	0.94	(-0.19 / +0.21)
20	2059.04	(-1.49 / +1.49)	0.97	(-0.21 / +0.22)
21	2101.88	(-1.66 / +1.66)	0.79	(-0.19 / +0.19)
22	2146.16	(-1.32 / +1.22)	0.74	(-0.16 / +0.18)
23	2188.69	(-2.23 / +2.39)	0.55	(-0.15 / +0.15)
24	2233.96	(-2.03 / +1.87)	0.56	(-0.15 / +0.15)
25	2279.03	(-1.96 / +41.67)	0.84	(-0.41 / +0.24)
26	2322.60	(-44.02 / +2.06)	0.38	(-0.16 / +0.39)
27	2362.40	(-2.74 / +2.06)	0.50	(-0.15 / +0.15)
28	2403.61	(-1.58 / +1.43)	0.46	(-0.14 / +0.14)

τ [d]	σ_τ	η [μHz]	σ_η	
all	0.47	(-0.04 / + 0.06)	7.8	(-0.8 / +0.8)

b [ppm ² / μHz]	σ_b
all	(-0.02/ + 0.02)

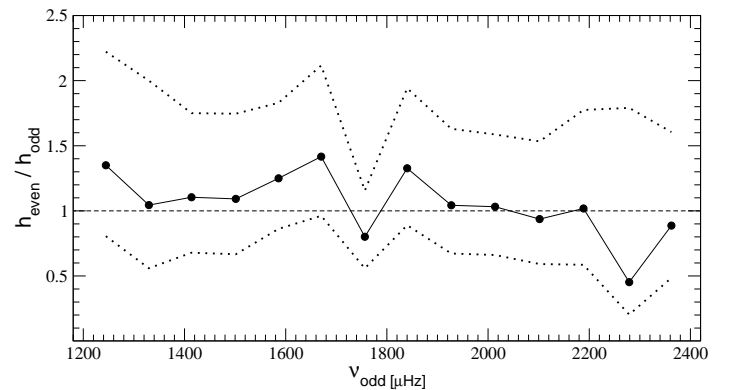


Fig. 10. The mode height ratios for subsequent modes listed in Tab. 5 (e.g., h_{P2}/h_{P1}) are shown as filled circles. The dotted lines correspond to the 68.2% confidence limits. The dashed line indicates a height ratio of unity. The outlier at $\sim 2280 \mu\text{Hz}$ is due to profiles 25 and 26, which are ambiguous detections.

plexity when fitting real observations. Our analysis of HD 49933 paints a slightly different picture of its pulsation spectrum, compared to Appourchaux et al. (2008), as we do not find $\ell = 2$ modes. We failed to gather any convincing evidence for rotational splitting in the data, possibly due to the low SNR. The picture presented by Fig. 10 is inconclusive concerning the mode identification given in Appourchaux et al. (2008). Comparing their findings to ours, their $\ell = 1$ modes correspond to the even profiles listed in Tab. 5. Overall, these profiles show a slight excess in power compared to the odd profiles. However, we think that the uncertainties are too large to make a definite statement about the mode identification. We will investigate this important issue in a forthcoming paper (Kallinger et al. 2008a).

In general, it is important to keep in mind that actually present model components which we argue to be unresolved in the data undoubtedly contribute to the power in the spectrum, influencing the parameter estimation process. For instance, it might be possible that unresolved rotational splitting leads to overestimated linewidths, which complicates the analysis of mode lifetimes across the spectrum. Also, the presence of unresolved modes might introduce a systematic error in the detection of adjacent modes, i.e., shift the centroids of their profiles. So far, we can only judge from the shapes of the parameters' marginal distributions whether the models are sufficiently complex for the data, as well as use false-alarm tests in order to not over-interpret. The simple 2-profile model, which was used to determine the values presented in Tab. 5, satisfies this balance.

With improving data quality, when there is evidence for additional and/or closely spaced modes, it might be advantageous to change the model by combining the corresponding Lorentzian profiles and fitting them as a group, similar to our approach to rotational splitting. In this case, instead of treating the profile frequencies as independent, only one frequency parameter and a number of frequency difference parameters should be fitted, so that the various profiles won't overlap. Using independent mode heights, and only constraining the frequency differences in terms of their sign, will again yield an unbiased result without the need of prior mode identification. We stress, however, that only with the mode height prior the influence of noise can be treated properly and the danger of over-fitting lowered, no matter which kind of model is used, unless some other suited likelihood function is found.

It would also be interesting to implement parallel tempering (PT). With increasing complexity of the p-mode profile model, this also prevents the MCMC algorithm from getting stuck in local maxima and fail to cover the whole parameter range of interest. In addition, PT could also be used to perform model selection by calculating the global likelihood of a model via integration over the tempering parameter (see, e.g., Gregory 2007). However, we think that the validity of applying this kind of model selection to p-mode analysis needs to be carefully tested first.

Acknowledgements. We would like to especially thank Daniel Huber (Sydney Institute for Astronomy, Sydney, Australia) for interesting discussions. We also thank David Guenther (Department of Astronomy and Physics, Halifax, Canada), Peter Reegen (Institute for Astronomy, Vienna, Austria) and Tim Bedding (Sydney Institute for Astronomy, Sydney, Australia) for their suggestions. MG, TK and WW have received financial support by the Austrian Fonds zur Förderung der wissenschaftlichen Forschung (P17890-N02). Last but not least, we are very thankful for the constructive comments provided by the anonymous referee who helped to greatly improve this article. We are grateful for the VIRGO data being publicly available.

References

- Aigrain, S., Favata, F., & Gilmore, G. 2004, *A&A*, 414, 1139
 Appourchaux, T. 2008, *Astronomische Nachrichten*, 329, 485
 Appourchaux, T., Andersen, B., & Sekii, T. 2002, in *ESA Special Publication*, Vol. 508, *From Solar Min to Max: Half a Solar Cycle with SOHO*, ed. A. Wilson, 47–50
 Appourchaux, T., Gizon, L., & Rabello-Soares, M.-C. 1998, *A&AS*, 132, 107
 Appourchaux, T., Michel, E., Auvergne, M., et al. 2008, *A&A*, 488, 705
 Baglin, A., Michel, E., Auvergne, M., et al. 2006, in *ESA Special Publication*, Vol. 1306, *ESA Special Publication*, 39–50
 Bedding, T. & Kjeldsen, H. 2006, in *ESA Special Publication*, Vol. 624, *Proceedings of SOHO 18/GONG 2006/HELAS I, Beyond the spherical Sun*
 Benomar, O. 2008, *Communications in Asteroseismology*, 157, 98
 Brewer, B. J., Bedding, T. R., Kjeldsen, H., & Stello, D. 2007, *ApJ*, 654, 551
 Chaplin, W. J., Elsworth, Y., Howe, R., et al. 1997, *MNRAS*, 287, 51
 Croll, B. 2006, *PASP*, 118, 1351
 Fröhlich, C., Crommelynck, D. A., Wehrli, C., et al. 1997, *Sol. Phys.*, 175, 267
 Gregory, P. C. 2005, *Bayesian Logical Data Analysis for the Physical Sciences: A Comparative Approach with 'Mathematica' Support* (Bayesian Logical Data Analysis for the Physical Sciences: A Comparative Approach with 'Mathematica' Support. Edited by P. C. Gregory. ISBN 0 521 84150 X (hardback); QA279.5.G74 2005 519.5'42 – dc22; 200445930. Published by Cambridge University Press, Cambridge, UK, 2005.)
 Gregory, P. C. 2007, *MNRAS*, 374, 1321
 Harvey, J. 1985, in *ESA Special Publication*, Vol. 235, *Future Missions in Solar, Heliospheric & Space Plasma Physics*, ed. E. Rolfe & B. Battrock, 199–+
 Kallinger, T., Gruberbauer, M., Guenther, D. B., Fossati, L., & Weiss, W. W. 2008a, *ArXiv e-prints*, 0811.4686
 Kallinger, T., Weiss, W. W., Barban, C., et al. 2008b, *A&A*, submitted
 Michel, E., Samadi, R., Baudin, F., et al. 2008, *ArXiv e-prints* (0809.1078)
 Reegen, P. 2007, *A&A*, 467, 1353
 Roberts, G. O., Gelman, A., & Gilks, W. R. 1997, *Ann. Appl. Prob.*, 7, 110

List of Objects

'HD 49933' on page 1